J Eng Math (2007) 62:173–188
DOI 10.1007/s10665-007-9203-1

Transformation of flexural gravity waves by heterogeneous boundaries

Joydip Bhattacharjee · Debabrata Karmakar · Trilochan Sahoo

Received: 14 December 2006 / Accepted: 16 October 2007 / Published online: 16 November 2007

Abstract The transformation of flexural gravity waves due to wave scattering by heterogeneous boundaries is investigated under the assumption of the linearized water-wave theory. The heterogeneous boundaries include step-type bottom topography as well as heterogeneity in the material property of a floating ice-sheet. By applying the generalized expansion formulae along with the corresponding orthogonal mode-coupling relations, the boundary-value problem (BVP) is reduced to linear system of algebraic equations. The system of equations is solved numerically to determine the full solution of the problem under consideration. Energy relations are derived and used to check the accuracy of the computational results of the scattering problem. Explicit relations for the shoaling and scattering coefficients due to the change in water depth and heterogeneous ice-sheet are derived. These derivations are based on the law of conservation of energy flux under the assumptions of the linearized shallow-water theory. The change in water depth and the structural characteristics of the medium significantly contribute to the change in the scattering and shoaling coefficients and the deflection of the structure. The present results are likely to play a significant role in the analysis of flexural gravity-wave propagation in problems of variable topography for which a direct computational approach is being utilized.

Keywords Flexural gravity waves · Reflection and transmission coefficients · Shallow-water approximations · Variable topography

1 Introduction

The study on wave interaction with floating ice sheets was started by Greenhill [1]. However, major scientific investigations on various issues regarding Antarctica has significantly progressed world-wide since 1957/1958, the International Geophysical Year. Wave–ice interactions are very important in the Marginal Ice Zones (MIZ) since the waves cause fractures in the continuous ice. Simultaneously, the region of broken ice scatters wave energy protecting the interior of the ice from further wave-induced fracture. In the Antarctic regions, as the wave from the open ocean penetrates into the ice shelf, it experiences an impedance change due to the flexural properties of the structure. In addition, there are several irregularities in the medium such as the ice leads being either open or refrozen, pressure ridges and certain physical and mechanical changes in the properties of the sea ice. In addition, the

J. Bhattacharjee · D. Karmakar · T. Sahoo (✉)
Department of Ocean Engineering and Naval Architecture, Indian Institute of Technology, Kharagpur 721 302, India
e-mail: tsahoo@naval.iitkgp.ernet.in; tsahoo1967@yahoo.com

ice-covered regions are often extended up to continental shelves in the polar regions where topographic variation is often observed. These irregularities result in altering the dispersion relation and hence transformation of the waves takes place below the ice sheet [2].

The recent interest in ocean-wave interaction with large floating structures is largely due to the growing importance to utilize the ocean space for various humanitarian activities and military operations. The construction of floating airports, floating cities, floating army bases, etc. has advantages over the conventional land-reclamation processes. These structures are easy to construct, handle and remove, and has little environmental impact on the country and the neighboring countries' coastline and the marine eco-system. In general, the thickness of these kinds of structures is negligible (<10 m) compared to the length of the structures (in the order of kilometers). In the literature, these floating ice sheets and the large floating structures are modelled as thin floating elastic plates. Thus, the thin-plate model of Euler–Bernoulli is in general used for the structural parts in the mathematical formulation of the BVP. Because of the commonality of the two classes of problems, the study on wave interaction with large floating structures plays a vital role in both Marine technology and Arctic engineering.

Interaction of surface gravity waves with flexible floating structures gives rise to the flexural gravity waves. This branch is well studied in homogeneous fluid media having uniform water depth. Various analytical and numerical methods are being developed in the literature to handle such problems. Most of these works can be found in the classical works presented [3–6] and the literature cited therein. In addition, the significant progress in the literature on wave interaction with flexible floating structures in homogeneous fluid and structural medium in the case of uniform water depth is reviewed by Watanabe et al. [7] and Chen et al. [8]. However, most of these floating flexible structures are constructed near the offshore region, where the bottom topography is usually uneven. Often it is difficult to find vast areas having flat sea bed in the coastal region where large floating structures are being constructed. Further, the concept of flexural gravity-wave propagation over heterogeneous boundaries is an important phenomenon in the continental shelf in the two polar regions. In this context it is important to analyze the behavior of flexural gravity waves with change in bottom topography and heterogeneity in structural medium.

The topographic variation is very common in most of the ocean-wave propagation problems. Even for the simplest of such problems, like wave scattering by a sudden change in bottom topography, one has to take recourse to approximate solutions. In the last few decades, significant progress has been made in the literature to develop various approximate solution approaches. Newman [9] presented theoretical and experimental results for free-surface gravity-wave scattering by an infinite step and various other cases are well described in [10, Sect. 2.6]. To deal with wave scattering by variable topography, one of the most widely used methods is based on the mild-slope approximation developed by Berkhoff [11]. Rhee [12,13] analyzed the scattering of surface gravity waves by stepwise obstacles. Ehrenmark [14] analyzed the classical problem of oblique-wave incidence on a plane beach by the application of integral transforms. Most of these studies are related to surface gravity waves. On the other hand, recent emphasis on flexural gravity waves is on problems involving heterogeneous boundaries. Sturova [15] analyzed the deflection of floating flexible platforms in shallow water. Wang and Meylan [16] presented a solution for the linear wave forcing of a floating thin elastic plate on water of variable depth by the combined application of boundary-element and integral-equation methods. Andrianov and Hermans [17] discussed the influence of water depth on the hydro-elastic response of very large floating structures. They obtained the results for the reflection and transmission coefficients by analyzing an integro-differential equation. Recently, Williams and Squire [2,18] analyzed scattering due to a change in structural characteristics of a floating structure. Porter and Porter [19] analyzed the effect of a change in water depth and thickness of a structure based on mild-slope approximations. Belibassakis and Athanassoulis [20] performed a hydro-elastic analysis of large floating platforms over variable bathymetry by a coupled-mode method.

In the present paper, the scattering of flexural gravity waves by an abrupt change in water depth and structural heterogeneity is analyzed for water of finite depth. The analysis is based on the expansion formulae and the orthogonal mode-coupling relations developed by Manam et al. [6] which is equivalent to that developed by Lawrie and Abrahams [21]. However, an alternate and straightforward derivation of the expansion formula for finite depth is given in Appendix by a suitable application of the Fourier-sine transform technique and Cauchy integral theorem of complex-function theory. The energy relation associated with flexural gravity-wave scattering is derived by two

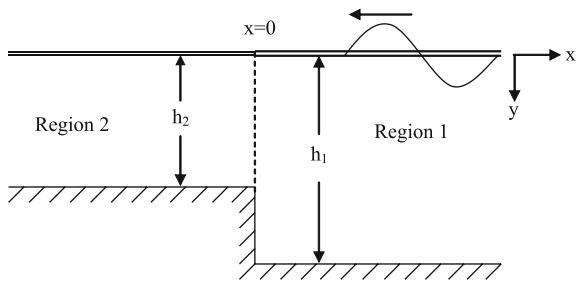

Fig. 1 Schematic diagram

alternate approaches. Using linearized shallow-water theory, we derive explicit expressions for the reflection and transmission coefficients considering continuity of the surface elevation and the law of conservation of energy flux. Explicit relations for shoaling coefficients are also obtained based on the law of conservation of energy flux. Simple numerical computations are performed to analyze the hydro-elastic response of floating flexible structures over uneven bottom topography and change in material characteristics of the structure.

2 Wave transformation by heterogeneous boundaries

Transformation of flexural gravity waves takes place due to various physical processes which have an adverse effect on the wave characteristics and the associated floating structure. In the context of the present study, emphasis is put on wave transformation due to the change in bottom topography, thickness and rigidity of the floating structure. The floating structure is considered as a large floating ice sheet and the problem is analyzed in a two-dimensional Cartesian co-ordinate system.

2.1 The general boundary-value problem

In the present subsection, the general BVP is formulated under the assumption of the linearized water-wave theory. The floating ice sheet is modeled as an Euler–Bernoulli beam equation. The fluid is assumed to occupy the regions $0 < x < \infty, 0 < y < h_1$ (referred as region 1) and $-\infty < x < 0, 0 < y < h_2$ (referred as region 2). We consider an infinite ice-sheet floating on the upper surface of the fluid. The ice-sheet is given an abrupt change in the constituent ice-material from $E_1 I_1$ to $E_2 I_2$ and water depth from h_1 to h_2 at $x = 0$ as in Fig. 1. We assume that the fluid is inviscid, incompressible and that the motion is irrotational and simply harmonic in time with angular frequency ω. These assumptions ensure the existence of a velocity potential $\Phi_j(x, y, t)$ of the form $\Phi_j(x, y, t) = \mathfrak{Re}\{\phi_j(x, y)\mathrm{e}^{-\mathrm{i}\omega t}\}$. Further, it is assumed that the deflection of the ice-sheet is simple harmonic in time with frequency ω which gives rise to the ice deflection $\zeta_j(x, t)$ of the form $\zeta_j(x, t) = \mathfrak{Re}\{\eta_j(x)\mathrm{e}^{-\mathrm{i}\omega t}\}$. Thus, the spatial velocity potential $\phi_j(x, y)$ satisfies the Laplace equation as given by

$$\nabla^2 \phi_j = 0 \quad \text{in the fluid domain.} \tag{1}$$

The linearized kinematic and dynamic boundary conditions in the jth region on the mean free surface $y = 0$ are given by

$$\frac{\partial \phi_j}{\partial y} + \mathrm{i}\omega\eta_j = 0, \tag{2}$$

$$\omega^2 \rho_j d_j \eta_j = E_j I_j \frac{\partial^4 \eta_j}{\partial x^4} + P_j(x, 0), \tag{3}$$

where the pressure is obtained from Bernoulli's equation as

$$P_j = \mathrm{i}\rho\omega\phi_j + \rho g \eta_j. \tag{4}$$

Combining the kinematic and dynamic boundary conditions (2–4), we obtain the boundary condition on the ice-covered mean free surface $y = 0$ as

$$\left(c_{j0} + c_{j1}\frac{\partial^4}{\partial x^4}\right)\frac{\partial \phi_j}{\partial y} + d_{j0}\phi_j = 0 \quad \text{on } y = 0, \tag{5}$$

with $c_{j0} = 1$, $c_{j1} = E_j I_j/\{\rho g - \rho_j d_j \omega^2\}$, $d_{j0} = \rho\omega^2/\{\rho g - \rho_j d_j \omega^2\}$, $I_j = d_j^3/12(1-\nu_j^2)$, E_j = Young's modulus, ν_j = Poisson's ratio, ρ = density of water, ρ_j = density of the ice-sheet, g = acceleration due to gravity and d_j = thickness of the ice-sheet. The bottom boundary condition for this case becomes

$$\frac{\partial \phi}{\partial n} = 0 \quad \text{on } \{y = h_2, -\infty < x < 0\} \cup \{y = h_1, 0 < x < \infty\} \cup \{x = 0, h_2 < y < h_1\}, \tag{6}$$

where n is the outward-drawn normal to the bottom boundary. Finally, the general form of the far-field condition is

$$\begin{aligned} \phi_1(x, y) &\sim \frac{\cosh k_{10}(h_1 - y)}{\cosh k_{10} h_1}\{a_{11}\mathrm{e}^{-\mathrm{i}k_{10}x} + a_{12}\mathrm{e}^{\mathrm{i}k_{10}x}\} \quad \text{as } x \to \infty \\ \phi_2(x, y) &\sim \frac{\cosh k_{20}(h_2 - y)}{\cosh k_{20} h_2}\{a_{21}\mathrm{e}^{-\mathrm{i}k_{20}x} + a_{22}\mathrm{e}^{\mathrm{i}k_{20}x}\} \quad \text{as } x \to -\infty, \end{aligned} \tag{7}$$

with $a_{lj}, l, j = 1, 2$ being the far-field wave amplitudes which depend upon the nature of the physical problem under consideration. The roots k_{j0}, $j = 1, 2$ are real and positive and satisfy the dispersion relations

$$d_{j0} = (c_{j1}k_{j0}^4 + c_{j0})k_{j0}\tanh k_{j0}h_j, \quad j = 1, 2. \tag{8}$$

2.2 Wave scattering due to heterogeneous boundaries

In case of wave scattering due to an abrupt change in bottom topography (often referred to as a step) and material properties of the structure as in Fig. 1, $\phi_j(x, y)$ with $j = 1, 2$ satisfy Eq. (1). In addition, it satisfies the boundary conditions (2–7) with $a_{11} = 1$, $a_{12} = R_0$, $a_{21} = T_0$ and $a_{22} = 0$ in (7). Here, R_0 and T_0 are associated with the amplitude of the reflected and transmitted waves. The continuity of velocity and pressure at the interface $x = 0$ yields

$$\phi_{2x}(0, y) = \phi_{1x}(0, y), \ \phi_2(0, y) = \phi_1(0, y), \quad \text{in } 0 < y < h_2. \tag{9}$$

Near the edge of the two interface points $(0\pm, 0)$ at the mean free surface, it is assumed that the plate deflection, slope of deflection, bending moment and shear force are continuous, which yield

$$\begin{aligned} &\phi_{1y}(0+, 0) = \phi_{2y}(0-, 0) = \alpha_1 \text{ (say)}, \ \ \phi_{1xy}(0+, 0) = \phi_{2xy}(0-, 0) = \alpha_2 \text{ (say)}, \\ &E_1 I_1 \phi_{1yyy}(0+, 0) = E_2 I_2 \phi_{2yyy}(0-, 0) = \alpha_3 \text{ (say)}, \ E_1 I_1 \phi_{1xyyy}(0+, 0) = E_2 I_2 \phi_{2xyyy}(0-, 0) = \alpha_4 \ \ \text{(say)}. \end{aligned} \tag{10}$$

Using the expansion formula for the flexural gravity wavemaker problem as in [6] (An alternate straightforward derivation of a generalized expansion will be discussed in Appendix), the ϕ_j, $j = 1, 2$ are expanded as

$$\begin{aligned} \phi_1(x, y) &= (\mathrm{e}^{-\mathrm{i}k_{10}x} + R_0\mathrm{e}^{\mathrm{i}k_{10}x})f_{10}(y) + \sum_{n=I}^{II} R_n \mathrm{e}^{\mathrm{i}\epsilon_n k_{1n}x} f_{1n}(y) + \sum_{n=1}^{\infty} R_n \mathrm{e}^{-k_{1n}x} f_{1n}(y), \quad x > 0, \\ \phi_2(x, y) &= T_0\mathrm{e}^{-\mathrm{i}k_{20}x} f_{20}(y) + \sum_{n=I}^{II} T_n \mathrm{e}^{-\mathrm{i}\epsilon_n k_{2n}x} f_{2n}(y) + \sum_{n=1}^{\infty} T_n \mathrm{e}^{k_{2n}x} f_{2n}(y), \qquad\qquad x < 0, \end{aligned} \tag{11}$$

where R_0, T_0, R_n, T_n, $n = I, II, 1, 2, \ldots$, are unknown constants to be determined, $\epsilon_n = 1$ for $n = I, 0, 1, 2, \ldots$ and $\epsilon_{II} = -1$. The eigenfunctions f_{jn} are given by

$$f_{jn}(y) = \frac{\cosh k_{jn}(h_j - y)}{\cosh k_{jn} h_j}, \ \ n = 0, I, II \ \text{ and } \ f_{jn}(y) = \frac{\cos k_{jn}(h_j - y)}{\cos k_{jn} h_j}, \ \ n = 1, 2 \ldots \tag{12}$$

with the eigenvalues k_{jn}'s satisfying the dispersion relation

$$d_{j0} = (c_{j1}k_{jn}^4 + c_{j0})k_{jn}\tanh k_{jn}h_j, \quad n = 0, I, II \tag{13}$$

and $k_{jn} = ik_{jn}$ for $n = 1, 2, 3, \ldots$. The dispersion relation for each $j = 1, 2$ in (13) has one real positive root k_{j0}, four complex roots $k_{jn}, n = I, II, \ldots, IV$ in the four quadrants and an infinite number of purely imaginary roots $k_{jn}, n = 1, 2, \ldots$. In our study, we have considered the two complex roots with positive real parts for the sake of boundedness of the solution. The terms containing the other complex roots do not contribute to the solution. Further, the eigenfunctions $f_{jn}(y)$ satisfy the orthogonal mode-coupling relation as given in [6] or as in Appendix:

$$\langle f_{jm}, f_{jn}\rangle = \int_0^{h_j} f_{jm}f_{jn}\mathrm{d}y + \frac{c_{j1}}{d_{j0}}\left\{f_{jm}'''(0)f_{jn}'(0) + f_{jm}'(0)f_{jn}'''(0)\right\}, \tag{14}$$

which satisfies,

$$\langle f_{jm}, f_{jn}\rangle = \begin{cases} 0 & \text{for} \quad m \neq n, \\ \dfrac{2k_{jn}h_j(c_{j0} + c_{j1}k_{jn}^4) + (c_{j0} + 5c_{j1}k_{jn}^4)\sinh 2k_{jn}h_j}{4k_{jn}(c_{j0} + c_{j1}k_{jn}^4)\cosh^2 k_{jn}h_j} & \text{for} \quad m = n = 0, I, II, \\ \dfrac{2k_{jn}h_j(c_{j0} + c_{j1}k_{jn}^4) + (c_{j0} + 5c_{j1}k_{jn}^4)\sin 2k_{jn}h_j}{4k_{jn}(c_{j0} + c_{j1}k_{jn}^4)\cos^2 k_{jn}h_j} & \text{for} \quad m = n = 1, 2\ldots. \end{cases}.$$

In order to determine the unknown coefficients, the above mode-coupling relation is applied to $\phi_2(0, y)$ and $f_{2m}(y)$ along with the continuity of pressure across the vertical interface $x = 0$, $0 < y < h_2$. Thus, from the second condition of (9) and the relation (14), we obtain

$$\begin{aligned}\langle \phi_2(0, y), f_{2m}(y)\rangle &= \int_0^{h_2} \phi_2(0, y)f_{2m}(y)\mathrm{d}y + \frac{c_{21}}{d_{20}}\left\{\phi_{2yyy}(0, 0)f_{2m}'(0) + \phi_{2y}(0, 0)f_{2m}'''(0)\right\} \\ &= \int_0^{h_2} \phi_1(0, y)f_{2m}(y)\mathrm{d}y + \frac{c_{21}}{d_{20}}\left\{\frac{\alpha_3}{E_2I_2}f_{2m}'(0) + \alpha_1 f_{2m}'''(0)\right\}\end{aligned} \tag{15}$$

for $m = 0, I, II, 1, 2, \ldots$. Using relation (11) in (15), we further obtain

$$\begin{aligned}&R_0\int_0^{h_2} f_{10}(y)f_{2m}(y)\mathrm{d}y + \sum_{n=I}^{II} R_n\int_0^{h_2} f_{1n}(y)f_{2m}(y)\mathrm{d}y + \sum_{n=1}^{\infty} R_n\int_0^{h_2} f_{1n}(y)f_{2m}(y)\mathrm{d}y \\ &\quad -T_m\langle f_{2m}(y), f_{2m}(y)\rangle - \alpha_1\frac{k_{2m}^3c_{21}}{d_{20}}\tanh k_{2m}h_2 - \alpha_3\frac{k_{2m}c_{21}}{E_2I_2d_{20}}\tanh k_{2m}h_2 = -\int_0^{h_2} f_{10}(y)f_{2m}(y)\mathrm{d}y.\end{aligned} \tag{16}$$

Once again, we apply the mode-coupling relation to $\phi_{1x}(0, y)$ and $f_{1m}(y)$ along with the continuity of the horizontal velocity across $x = 0$, $0 < y < h_2$ and the condition of zero horizontal velocity on $x = 0$, $h_2 < y < h_1$. Thus, from (6), along with the first condition of (9) and the relation (14), we obtain

$$\begin{aligned}\langle \phi_{1x}(0, y), f_{1m}(y)\rangle &= \int_0^{h_1} \phi_{1x}(0, y)f_{1m}(y)\mathrm{d}y + \frac{c_{11}}{d_{10}}\left\{\phi_{1xyyy}(0, 0)f_{1m}'(0) + \phi_{1xy}(0, 0)f_{1m}'''(0)\right\} \\ &= \int_0^{h_2} \phi_{2x}(0, y)f_{1m}(y)\mathrm{d}y + \frac{c_{11}}{d_{10}}\left\{\frac{\alpha_4}{E_1I_1}f_{1m}'(0) + \alpha_2 f_{1m}'''(0)\right\}\end{aligned} \tag{17}$$

for $m = 0, I, II, 1, 2, \ldots$. Using relation (11) in (17), we further obtain

$$\begin{aligned}&\mathrm{i}\epsilon_m k_{1m}R_m\langle f_{1m}(y), f_{1m}(y)\rangle + \mathrm{i}k_{20}T_0\int_0^{h_2} f_{20}(y)f_{1m}(y)\ \mathrm{d}y + \sum_{n=I}^{II}\mathrm{i}k_{2n}\epsilon_n T_n\int_0^{h_2} f_{2n}(y)f_{1m}(y)\ \mathrm{d}y \\ &\quad -\sum_{n=1}^{\infty} k_{2n}T_n\int_0^{h_2} f_{2n}(y)f_{1m}(y)\mathrm{d}y + \alpha_2\frac{k_{1m}^3c_{11}}{d_{10}}\tanh k_{1m}h_1 + \alpha_4\frac{k_{1m}c_{11}}{E_1I_1d_{10}}\tanh k_{1m}h_1 = \delta_m\end{aligned} \tag{18}$$

where

$$\delta_m = \begin{cases} \mathrm{i}k_{1m}\langle f_{1m}(y), f_{1m}(y)\rangle & \text{for} \quad m = 0, \\ 0 & \text{for} \quad m = I, II, 1, 2\ldots \end{cases}$$

and ϵ_n is same as defined earlier. Truncating the infinite series up to N terms, from (16) and (18), we obtain a linear system of $(2N+6)$ equations. Utilizing the continuity conditions for the plate deflection, slope of deflection, bending moment and shear forces at the origin, from (10) and (11) we obtain

$$T_0 k_{20} \tanh k_{20}h_2 + \sum_{n=I}^{II} T_n k_{2n} \tanh k_{2n}h_2 - \sum_{n=1}^{\infty} T_n k_{2n} \tan k_{2n}h_2 + \alpha_1 = 0, \tag{19a}$$

$$T_0 i k_{20}^2 \tanh k_{20}h_2 + \sum_{n=I}^{II} T_n i\epsilon_n k_{2n}^2 \tanh k_{2n}h_2 + \sum_{n=1}^{\infty} T_n k_{2n}^2 \tan k_{2n}h_2 - \alpha_2 = 0, \tag{19b}$$

$$T_0 k_{20}^3 \tanh k_{20}h_2 + \sum_{n=I}^{II} T_n k_{2n}^3 \tanh k_{2n}h_2 + \sum_{n=1}^{\infty} T_n k_{2n}^3 \tan k_{2n}h_2 + \frac{\alpha_3}{E_2 I_2} = 0, \tag{19c}$$

$$T_0 i k_{20}^4 \tanh k_{20}h_2 + \sum_{n=I}^{II} T_n i\epsilon_n k_{2n}^4 \tanh k_{2n}h_2 - \sum_{n=1}^{\infty} T_n k_{2n}^4 \tan k_{2n}h_2 - \frac{\alpha_4}{E_2 I_2} = 0. \tag{19d}$$

The above relations give four more equations in terms of $\alpha_1, \alpha_2, \alpha_3$, and α_4. Thus, we have obtained a system of $(2N+10)$ equations for the determination of $(2N+10)$ unknowns as given by R_0, R_I, R_{II}, $R_1, \ldots, R_n$, T_0, T_I, T_{II}, $T_1, \ldots, T_n$, $\alpha_1, \alpha_2, \alpha_3$, and α_4. The determination of the unknowns will in turn provide the velocity potentials in the respective fluid regions. Thus, the reflection and transmission coefficients K_r and K_t which are defined as

$$K_r = |R_0| \quad \text{and} \quad K_t = \left| \frac{k_{20} \tanh k_{20}h_2}{k_{10} \tanh k_{10}h_1} T_0 \right|, \tag{20}$$

are obtained once R_0 and T_0 have been computed. In the next subsection, the wave-energy relation for flexural gravity waves is derived for the scattering problem at hand.

2.3 Energy density and law of conservation of energy flux

Unlike the case of gravity waves, the average total flexural gravity-wave energy per unit surface area is the sum of average potential energy, kinetic energy and surface energy. In the present context, the surface energy is generated due to the deflection of the floating ice-sheet against the flexural rigidity of the ice-sheet. It is the same as the strain energy for an elastic plate (see [22, Sect. 4.2]). For a plane flexural gravity-wave profile $\zeta(x,t) = \mathfrak{Re}\left\{\frac{H}{2} e^{i(kx-\omega t)}\right\}$, the average potential energy $\mathcal{V}$, kinetic energy $\mathcal{T}$ and the surface energy $\mathcal{S}$ over one wave length are given by

$$\mathcal{V} = \frac{1}{L}\int_x^{x+L} \rho g(h+\zeta)\frac{(h+\zeta)}{2}\mathrm{d}x = \frac{1}{16}\rho g H^2, \tag{21}$$

$$\mathcal{T} = \frac{1}{L}\int_x^{x+L}\int_{-\eta}^{h} \frac{1}{2}\rho\left[\left(\frac{\partial\Phi}{\partial x}\right)^2 + \left(\frac{\partial\Phi}{\partial y}\right)^2\right]\mathrm{d}x\mathrm{d}y + \frac{\rho_{\mathrm{ice}} d}{2L}\int_x^{x+L}\left(\frac{\partial\zeta}{\partial t}\right)^2 \mathrm{d}x = \frac{1}{16}H^2(EIk^4 + \rho g), \tag{22}$$

and

$$\mathcal{S} = \frac{EI}{2L}\int_x^{x+L}\left(\frac{\partial^2\zeta}{\partial x^2}\right)^2 \mathrm{d}x = \frac{1}{16}H^2 EIk^4, \tag{23}$$

where the velocity potential $\Phi(x,y,t)$ is given by

$$\Phi(x,y,t) = \mathfrak{Re}\left\{\frac{iHg(EIk^4 + \rho g - \rho_{\mathrm{ice}} d\omega^2)}{2\omega}\frac{\cosh k(h-y)}{\cosh kh} e^{i(kx-\omega t)}\right\} \tag{24}$$

with ρ_{ice} being the density of the ice-sheet; d is the thickness of the ice-sheet, h is the finite water depth, H is the wave height and L is the wave length. Thus, the total energy density for flexural gravity waves is given by

$$\mathcal{E} = \mathcal{V} + \mathcal{T} + \mathcal{S} = \frac{1}{8}H^2(EIk^4 + \rho g). \tag{25}$$

Now, the average energy flux $\mathcal{F}$ over a time period is obtained as the product of the group velocity c_g and energy density $\mathcal{E}$, which yields

$$\mathcal{F} = \mathcal{E}c_g, \tag{26}$$

where the group velocity c_g is given by

$$c_g = nc, \tag{27}$$

with

$$n = \frac{1}{2}\left\{\frac{5EIk^4 + \rho g - \rho_{\text{ice}}d\omega^2}{EIk^4 + \rho g} + \frac{EIk^4 + \rho g - \rho_{\text{ice}}d\omega^2}{EIk^4 + \rho g}\frac{2kh}{\sinh 2kh}\right\},\ c = \sqrt{\frac{(EIk^4 + \rho g)\tanh kh}{k(\rho + \rho_{\text{ice}}dk\tanh kh)}}.$$

Next, we will derive the energy relation associated with the scattering of flexural gravity waves as in Sect. 2.2. Using conditions (2) and (7), we can derive that the surface displacement $\zeta_j(x,t)$ satisfies

$$\begin{aligned}
\zeta_1(x,t) &\sim \frac{H_{11}}{2}\mathrm{e}^{-\mathrm{i}(k_{10}x+\omega t)} + \frac{H_{12}}{2}\mathrm{e}^{\mathrm{i}(k_{10}x-\omega t)} \quad && \text{as } x \to \infty,\\
\zeta_2(x,t) &\sim \frac{H_{21}}{2}\mathrm{e}^{-\mathrm{i}(k_{20}x+\omega t)} && \text{as } x \to -\infty.
\end{aligned} \tag{28}$$

where the wave amplitudes H_{lj} are related to a_{lj} by the relation $a_{lj} = \{\mathrm{i}(E_lI_lk_{l0}^4 + \rho g - \rho_l d_l\omega^2)H_{lj}\}/\{2\rho\omega\}$ for $l, j = 1, 2$. Utilizing the law of conservation of energy flux as given by

$$\nabla\{\mathcal{E}c_g\} = 0, \tag{29}$$

from Eq. (28), we derive the energy relation as

$$1 - K_r^2 = \gamma\ K_t^2 \tag{30}$$

where

$$\gamma = \frac{k_{10}\sinh 2k_{10}h_1}{k_{20}\sinh 2k_{20}h_2}\frac{(\rho g - \rho_2 d_2\omega^2 + E_2I_2k_{20}^4)2k_{20}h_2 + (\rho g - \rho_2 d_2\omega^2 + 5E_2I_2k_{20}^4)\sinh 2k_{20}h_2}{(\rho g - \rho_1 d_1\omega^2 + E_1I_1k_{10}^4)2k_{10}h_1 + (\rho g - \rho_1 d_1\omega^2 + 5E_1I_1k_{10}^4)\sinh 2k_{10}h_1}. \tag{31}$$

The energy relation (30) is derived in an alternate manner by applying Green's identity on ϕ and its complex conjugate $\bar{\phi}$ (as in [3]), which yields

$$\oint_C \left(\phi\frac{\partial\bar{\phi}}{\partial n} - \bar{\phi}\frac{\partial\phi}{\partial n}\right) = 0. \tag{32}$$

In Eq. (32), C is the closed contour which consist of the horizontal upper surface ($-\infty < x < \infty; y = 0$), two vertical boundaries ($0 < y < h_2; x \to -\infty$) and ($0 < y < h_1; x \to \infty$) and the rigid bottom boundary $\{-\infty < x < 0; y = h_2\} \cup \{x = 0; h_2 < y < h_1\} \cup \{0 < x < \infty; y = h_1\}$. This alternate derivation also justifies the surface-energy term in the definition of total energy density. It may be noted that the kinetic-energy density is equal to the sum of the surface-energy density and the potential-energy density. The strain energy for flexural gravity waves is similar to the surface energy for capillary gravity waves (see [23, Sect. 15]).

3 Wave transformation based on shallow-water theory

In the context of the present paper, we will investigate the effect of shoaling and reflection due to changes in water depth and heterogeneity in the floating ice-sheet. The analysis is based on the law of conservation of energy flux

and pressure continuity at the interface. Under the assumption of the linearised shallow-water theory, the surface elevation and the velocity potential are related by the equation

$$\frac{\partial \eta}{\partial t} = h\frac{\partial^2 \phi}{\partial x^2}. \tag{33}$$

Combining Eqs. (3), (4), and (33) and neglecting the modified ice-draft term $\delta_j = \rho_j d_j/\rho$, we obtain the linearized long flexural gravity wave equation as [15]

$$D_j \frac{\partial^6 \phi_j}{\partial x^6} + \frac{\partial^2 \phi_j}{\partial x^2} = -\frac{\omega^2}{g h_j}\phi_j, \tag{34}$$

where $D_j = E_j I_j/\rho g$. The general form of the far-field behavior of a long flexural gravity wave is given by (28) (see [10, Sect. 2.6]). The eigenvalues k_{j0} in (28) are the positive real roots of the shallow-water flexural gravity-wave dispersion relation

$$(D_j k_{j0}^4 + 1)k_{j0}^2 = \frac{\omega^2}{g h_j}. \tag{35}$$

Apart from the positive real root, Eq. (35) has a negative real root and four complex roots. In the context of the present paper, we have given emphasis on the wave motion due to plane flexural gravity waves under shallow-water approximations. The wave heights $H_{lj},\ l = j = 1, 2$ in relation (28) depend on the type of physical problem under consideration. From (35), the phase and the group velocities c_j and c_{g_j} in case of shallow water are derived as $c_j = \sqrt{(D_j k_{j0}^4 + 1)g h_j},\ \ c_{g_j} = n_j c_j,\ \ n_j = (3D_j k_{j0}^4 + 1)/(D_j k_{j0}^4 + 1)$. Next, we will discuss the two cases of shoaling and reflection separately.

3.1 Case 1

In this case, we will assume that the wave is propagating from a region of uniform depth h_1 to a region of depth h_2 without any reflection and refraction. Then, the far-field behavior in relation (28) is satisfied with $H_{12} = 0$. Thus, the energy relation (30) yields

$$\frac{H_{21}}{H_{11}} = \left\{ \frac{1 + 3D_1 k_{10}^4}{1 + 3D_2 k_{20}^4} \frac{\sqrt{(1 + D_1 k_{10}^4)h_1}}{\sqrt{(1 + D_2 k_{20}^4)h_2}} \right\}^{\frac{1}{2}}. \tag{36}$$

This process is referred to as wave shoaling and the relation (36) will give the shoaling coefficient for plane flexural gravity waves. Relation (36) is the generalization of Green's law (as in [24, p. 138] for free-surface gravity waves) for flexural gravity waves.

3.2 Case 2

In this case we will consider the scattering of shallow-water waves due to a change in water depth. Thus, the general far-field condition (28) is satisfied and the energy relation as in (30) is satisfied with γ given by

$$\gamma = \frac{k_{10}}{k_{20}} \frac{1 + 3D_2 k_{20}^4}{1 + 3D_1 k_{10}^4}, \tag{37}$$

where $K_r = H_{12}/H_{11},\ \ K_t = H_{21}/H_{11}$. The continuity of the surface elevation at the point of heterogeneity at $x = 0$ yields

$$1 + K_r = K_t. \tag{38}$$

Combining Eqs. (30) and (38) with γ as in (37), we obtain the reflection and transmission coefficients for flexural gravity waves in shallow water as follows:

$$K_r = \frac{1 - \dfrac{1+3D_2k_{20}^4}{1+3D_1k_{10}^4}\dfrac{\sqrt{(1+D_2k_{20}^4)h_2}}{\sqrt{(1+D_1k_{10}^4)h_1}}}{1 + \dfrac{1+3D_2k_{20}^4}{1+3D_1k_{10}^4}\dfrac{\sqrt{(1+D_2k_{20}^4)h_2}}{\sqrt{(1+D_1k_{10}^4)h_1}}}, \quad K_t = \frac{2}{1 + \dfrac{1+3D_2k_{20}^4}{1+3D_1k_{10}^4}\dfrac{\sqrt{(1+D_2k_{20}^4)h_2}}{\sqrt{(1+D_1k_{10}^4)h_1}}}. \tag{39}$$

Here, it is observed that for $h_1 > h_2$ in the shallow-water approximation, $K_r \to 1$ and $K_t \to 2$. This case refers to the pure standing wave in region 1 and the transmitted wave is also a standing wave of the same wave height. On the other hand, the wave-height ratio in the case of no reflection as in (36) is due to the propagation of the progressive wave only (see [24, p. 144] for a comparison with the gravity-wave relation).

4 Numerical results and discussion

In the present context, the reflection and transmission coefficients are computed and analyzed with $E_j = 5\,\text{GPa}$, $\rho = 1025.0\,\text{kg m}^{-3}$, $\rho_j = 922.5\,\text{kg m}^{-3}$, $g = 9.81\,\text{m s}^{-2}$, and $\nu = 0.3$. In addition, the deflection of the ice-sheet ζ is computed and analyzed for several cases with $\omega t = 0$. For the purpose of computating K_r and K_t, the number of evanescent modes N is taken as 5. The conservation of wave energy for different cases is illustrated from the energy relation (30) in three different tables apart from the various computational results for K_r and K_t (Tables 1–3).

Figure 2 shows the variation of the reflection and transmission coefficients K_r and K_t versus the wave period T for different values of depth ratio h_2/h_1. It is observed that for the case when the region with lower water depth is nearer to the ice-covered surface, the reflection is higher and subsequently transmission is less. As T increases, K_r decreases to attain a minimum value and then starts increasing. This may be due to the change in phase of the reflected and transmitted waves. The reverse pattern is observed for K_t. It may be noted that in this case, the wave reflection is due to the abrupt change in the bottom topography as the ice-thickness is constant in both regions.

Table 1 Numerical check for the energy relation considering $h_2/h_1 = 0.75$ and $E_2/E_1 = 1.0$ with $T = 15\,\text{s}$

d_2/d_1	K_r	K_t	γ	$K_r^2 + \gamma K_t^2$
1.0	0.021554	0.973841	1.07451	1.01949
2.0	0.0996397	0.967477	1.08199	1.02269
3.0	0.931121	0.395638	1.1865	1.025271
4.0	0.982788	0.160043	1.18621	0.996256
5.0	0.915269	0.374003	1.18093	1.0029
6.0	0.914798	0.362066	1.17005	0.99024
7.0	0.940906	0.284258	1.15361	0.978519
8.0	0.961608	0.212024	1.13222	0.975588
9.0	0.974819	0.156699	1.10693	0.977452
10.0	0.983245	0.115129	1.07898	0.981072

Table 2 Numerical check for the energy relation considering $d_2/d_1 = 5$ and $E_2/E_1 = 1.0$ with $T = 15\,\text{s}$

h_2/h_1	K_r	K_t	γ	$K_r^2 + \gamma K_t^2$
0.05	1.00119	0.011952	16.6344	1.00475
0.25	0.965301	0.240528	3.20917	1.011747
0.50	0.966788	0.181746	1.60893	0.987825
0.75	0.915269	0.374003	1.18093	1.0029
1.0	0.937803	0.360006	1.00854	1.01019

Table 3 Numerical check for the energy relation considering $d_2/d_1 = 1$, $h_2/h_1 = 0.75$ and $E_2/E_1 = 1.0$

T (in sec)	K_r	K_t	γ	$K_r^2 + \gamma K_t^2$
5.0	0.0443708	1.00989	1.0	1.02185
7.5	0.0227061	0.990215	1.00021	0.981252
10.0	0.00850891	0.984246	1.01608	0.98439
12.5	0.0320499	0.974052	1.09436	1.03933
15.0	0.021554	0.973841	1.07451	1.01949

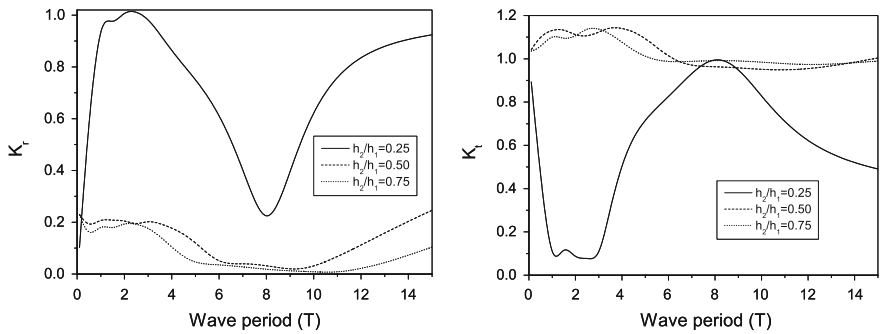

Fig. 2 Variation of K_r and K_t versus T for different h_2/h_1 with $d_2/d_1 = 1.0$

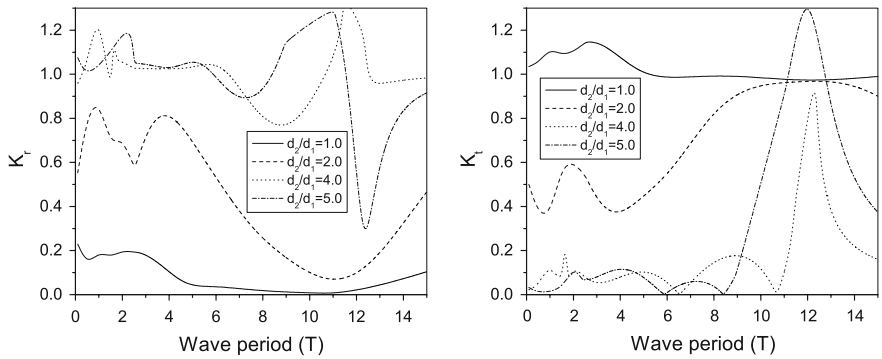

Fig. 3 Variation of K_r and K_t versus T for different d_2/d_1 with $h_2/h_1 = 0.75$

Figure 3 shows the variation of K_r and K_t versus the wave period for different values of the thickness ratio d_2/d_1. Here, it may be noted that there is a significant change in the reflection and transmission coefficients due to the abrupt change in thickness of the floating ice-sheets compared to the case $d_2 = d_1$. The reflection coefficient K_r is significantly higher when there is an abrupt change in water depth along with a change in thickness of the floating ice-sheet. This is due to the concentration of surface waves at the free surface. Thus, a change in the thickness of the structure is more effective compared to a change in water depth. Here, K_r initially increases with an increase in wave period T and attains a maximum and then decreases sharply to attain a minimum. In the intermediate range of wave periods from 5 to 12 s, the wave reflection is much less and remains almost unchanged. For wave periods longer than 12 s, K_r increases with T.

Figure 4 shows the change in the deflection of the ice-sheet ζ for different values of d_2/d_1. It is observed that, due to the scattering of the flexural gravity waves by the heterogeneity in the ice-sheet, as well as by the change in the bottom topography, the wave height and wave length have increased in the transmitted region. However, the vertical deflection decreases as the thickness of the ice-sheet increases.

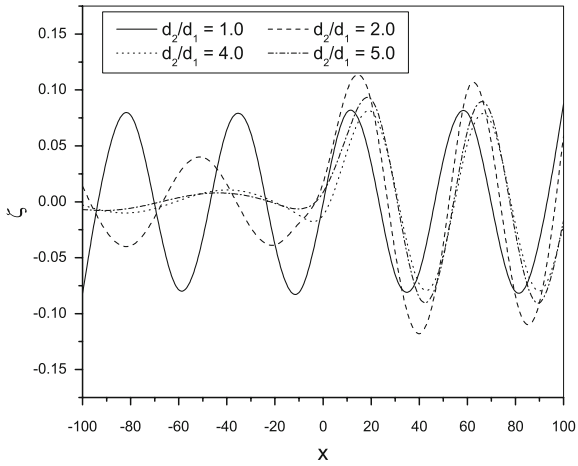

Fig. 4 Deflection of the ice-sheet ζ versus x (in meter) for various values of d_2/d_1 with $h_2/h_1 = 0.75$, $T = 5\,\mathrm{s}$

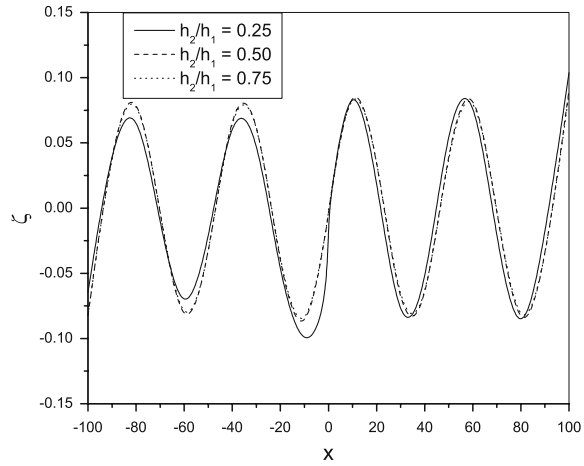

Fig. 5 Deflection of the ice-sheet ζ versus x (in meter) for various values of h_2/h_1 with $d_2/d_1 = 1.0$ $T = 5\,\mathrm{s}$

The deflection of the ice-sheet ζ versus x is plotted for different values of h_2/h_1 in Fig. 5 for the scattering of plane flexural gravity waves due to the change in water depth. It is observed that wave amplitude decreases in the transmitted region and it is comparatively higher in the region from which it is propagating. The increase in wave height may be due to the interaction of the incident waves with the reflected waves. However, with an increase in depth ratio h_2/h_1, the vertical-displacement amplitude increases.

In Fig. 6, the ratio between the wave heights H_2/H_1 is plotted versus T for different values of h_2/h_1 in the case of shoaling. It is clear from Fig. 6 that the incident wave height is greater than the transmitted wave height for waves with smaller wave periods. Further, as the wave period increases, the transmitted wave-height increases. For an intermediate value of the wave period, the incident and transmitted wave heights become equal. Afterwards the transmitted wave height becomes greater than the incident wave height. However, with an increase in h_2/h_1, H_2/H_1 increases for waves with relatively short time periods, whereas H_2/H_1 decreases with increasing h_2/h_1 for long period waves.

Figure 7 shows the variation of H_2/H_1 versus h_2/h_1 for different values of d_2/d_1 in the case of shoaling. It can be seen that, when $d_2/d_1 = 1.0$, H_2/H_1 approaches 1 as h_2/h_1 approaches 1. This is obvious, as there will be no wave transformation when there is no change in the water depth as well as the material property of the ice-sheet. As h_2/h_1 increases, initially H_2/H_1 starts increasing and attains a maximum value. After attaining the maximum, H_2/H_1 decreases gradually with increasing h_2/h_1.

In Figs. 8 and 9, the deflections of the ice-sheet ζ versus x are plotted for different values of h_2/h_1 and d_2/d_1, respectively, in the case of no reflection. Here, it is observed that when the waves propagate from higher to lower depth regions, the wave height increases and the wave length decreases. As h_2 increases, i.e., the bottom is far away from the upper surface, the wave height decreases. Figure 9 clearly shows that, as the thickness of the ice-sheet increases in the lower-depth region, the deflection of the ice-sheet decreases. This is so because, as the ice-thickness increases, the rigidity of the ice-sheet also increases resulting in less deflection.

Figure 10 shows the variation of the reflection and transmission coefficients K_r and K_t versus h_2/h_1 for different values of ice-thickness ratio d_2/d_1 in the case of reflection. It is observed that K_r and K_t initially increases with increasing h_2/h_1 to attain a maximum and then gradually decreases. In case $d_2/d_1 = 1$, as h_2/h_1 approaches 1, K_r tends to 0 and K_t tends to 1. It is also observed that, as d_2/d_1 decreases from 1, i.e., difference between the thickness of the two ice-sheets increases, K_r and K_t also increase. The graph for K_t in Fig. 10 shows a similar pattern as that of H_2/H_1 in Fig. 7, but the numerical values are higher in Fig. 7, which is when there is no reflection. This is because a part of the wave energy is reflected by the step wall.

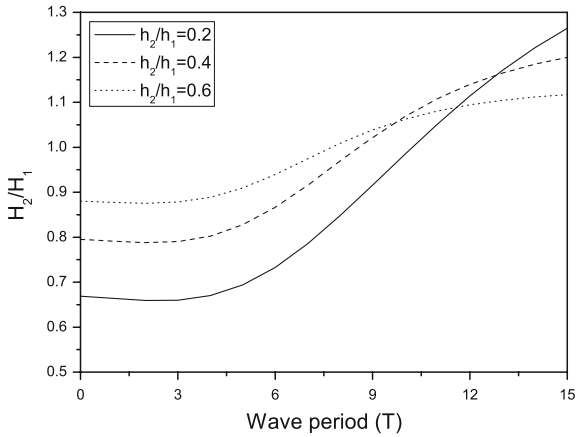

Fig. 6 H_2/H_1 versus T for different h_2/h_1 with $d_2/d_1 = 1.0$ in the case of shoaling

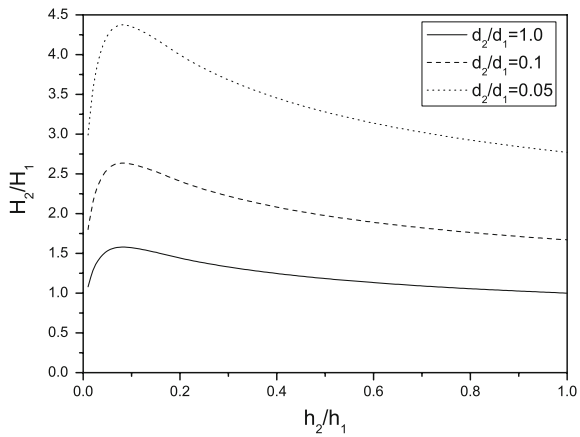

Fig. 7 H_2/H_1 versus h_2/h_1 for different d_2/d_1 with time period $T = 10$ s in the case of shoaling

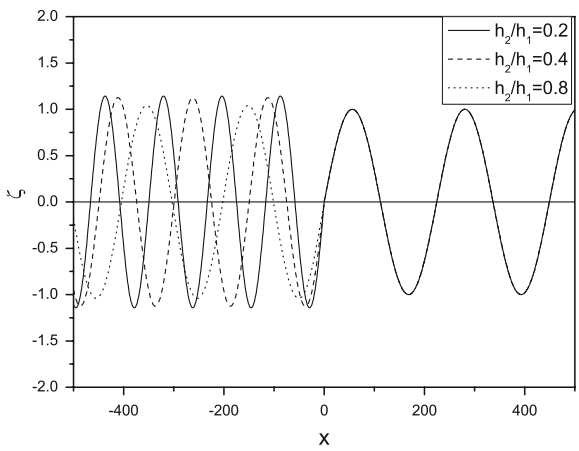

Fig. 8 Deflection of the ice-sheet ζ versus x (in meter) for various values of h_2/h_1 with $d_2/d_1 = 1.0$, $T = 10$ s in the case of shoaling

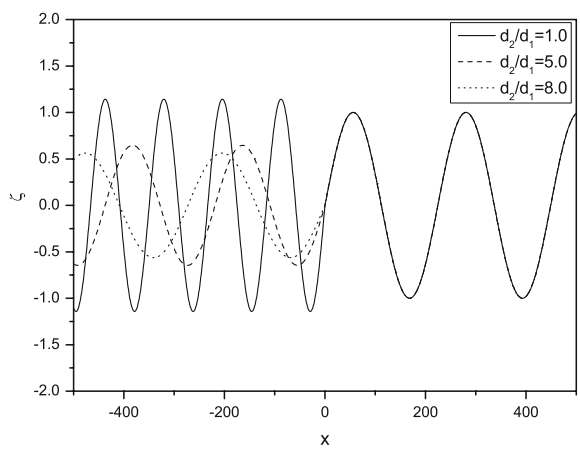

Fig. 9 Deflection of the ice-sheet ζ versus x (in meter) for various values of d_2/d_1 with $h_2/h_1 = 0.2$, $T = 10$ s in the case of shoaling

Figure 11 shows the variation of K_r and K_t versus the wave period T for different values of h_2/h_1. As T increases, K_r decreases and attains a minimum of zero at a particular time. After attaining the minimum, K_r increases with T. On the other hand, K_t increases with increasing wave period. It is also observed that the general behavior of K_r and K_t as h_2/h_1 increases in the case of shallow water is similar in nature with K_r and K_t in finite water depth as shown in Fig. 2. Further, the pattern of K_t is similar in nature with H_2/H_1 as in Fig. 6 but the numerical value is less due to the wave transformation by reflection.

Figures 12 and 13 show the variation of ζ versus x for different values of h_2/h_1 and d_2/d_1, respectively, for wave reflection in shallow water. The graphs show that the wave length in the transmitted region is less than that in the incident-wave region. On the other hand, the wave heights remain almost the same in both incident and transmitted regions. Further, an increase in the ice-thickness reduces the deflection of the ice-sheet.

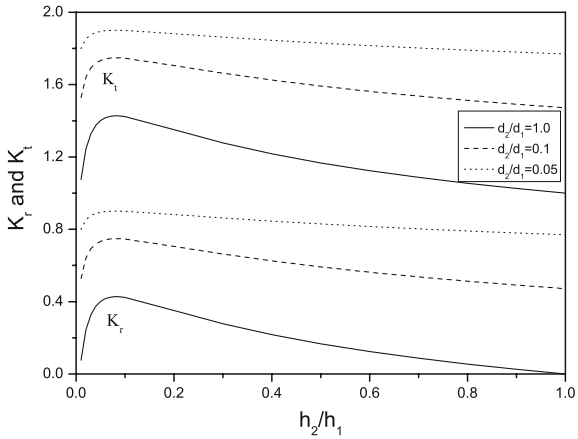

Fig. 10 K_r and K_t versus h_2/h_1 for different d_2/d_1 with time period $T = 10$ s in the case of reflection

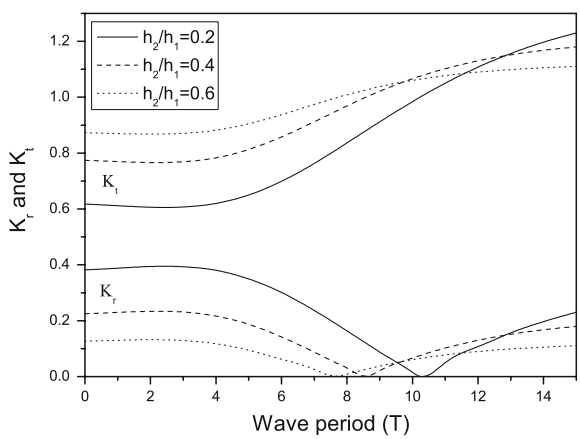

Fig. 11 K_r and K_t versus T for different h_2/h_1 with $d_2/d_1 = 1.0$ in the case of reflection

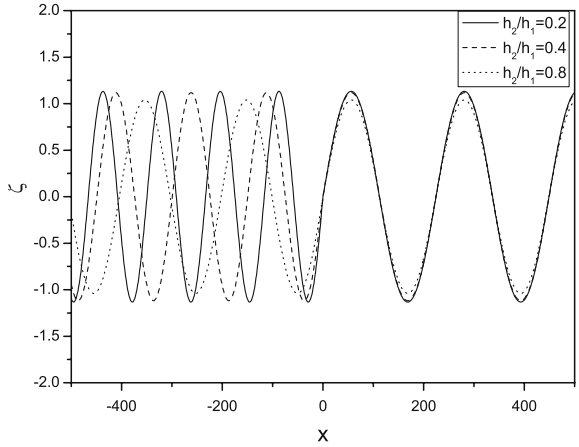

Fig. 12 Deflection of the ice-sheet ζ versus x (in meter) for various values of h_2/h_1 with $d_2/d_1 = 1.0$, $T = 10$ s in the case of reflection

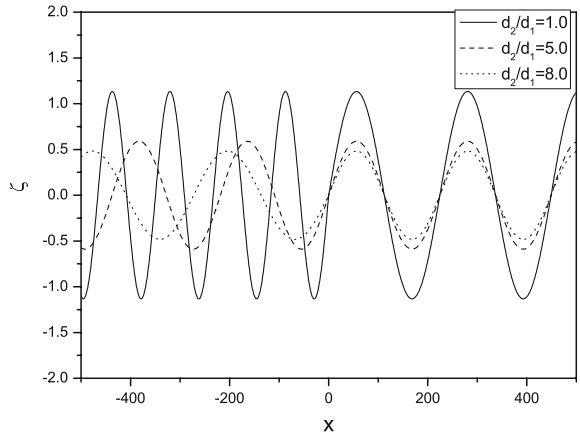

Fig. 13 Deflection of the ice-sheet ζ versus x (in meter) for various values of d_2/d_1 with $h_2/h_1 = 0.2$, $T = 10$ s in the case of reflection

5 Conclusions

In the present paper, energy relations for plane flexural gravity waves have been derived based on the law of conservation of energy flux. Further, the same relations are rederived by direct application of Green's second identity. The total energy density for flexural gravity waves is a combination of kinetic energy, potential energy and surface energy. The surface energy in this case is the strain energy due to the existence of the floating ice-sheet which is an additional surface apart from the free surface of water. Wave transformation due to change in water depth and heterogeneities in the floating ice has been investigated using the expansion formula for flexural gravity wavemaker problems. An alternate derivation of the expansion formula will be given in Appendix. The heterogeneity in the floating structure includes a change in the thickness of the ice-sheet along with the rigidity of the structure and is very common in the cold regions of the Arctic and Antarctic oceans. The change in the thickness results in variable flexural rigidity of the ice that leads to transformation of wave propagation. The effect of shoaling and reflection of plane flexural gravity waves has been analyzed based on the linearised theory of shallow-water waves. Explicit

expressions were obtained for the wave-height ratios for both shoaling and reflection. The results can be used as a numerical check for computational analysis of wave transformations due to complex bottom topography and structural heterogeneities.

In the present context, we discussed in detail the reflection and transmission coefficients and the deflections of the ice-sheet. We observed that, for waves with longer wave lengths, the reflection is more than for waves with shorter wave lengths. The numerical results also show that, due to the abrupt change in the bottom topography and structural heterogeneity of the floating ice-sheet, there is a significant change in the amplitude and length of the flexural gravity waves. These changes will lead to cracks in floating ice-sheets which, in turn, may break into small pieces. The results will be of importance in the field of Ocean Engineering in the design of mega floats and Cold Region Science and Technology apart from the application of the present method in different branches of Mathematical Physics.

Appendix: Alternate derivation of the generalized expansion formula

In this appendix, we provide an alternate derivation of the expansion formula associated with flexural gravity waves in finite water depth as in [6]. Karmakar et al. [25] presented the alternate derivation of the expansion formula for flexural gravity waves for infinite depth. In this case, the velocity potential $\phi(x, y)$ satisfies the Laplace equation as in (1) in the semi-infinite strip $0 < x < \infty, 0 < y < h$. The boundary condition on the structural boundary $y = 0$ is of the form

$$\mathcal{L}(\partial_x)\phi_y + \mathcal{M}(\partial_x)\phi = 0 \quad \text{on } y = 0,\ 0 < x < \infty, \tag{A1}$$

where $\mathcal{L}$ and $\mathcal{M}$ are the linear differential operators of the form $\mathcal{L}(\partial_x) = \sum_{n=0}^{n_0} c_n \partial_{x^{2n}}$, $\mathcal{M}(\partial_x) = \sum_{n=0}^{m_0} d_n \partial_{x^{2n}}$ with c_n's and d_n's are unknown constants. The far-field radiation condition is of the form

$$\phi(x, y) \sim \text{ multiple of } f_0(y)\mathrm{e}^{\mathrm{i}k_0 x} \quad \text{as } x \to \infty, \tag{A2}$$

where k_0 satisfies a relation in k given by

$$\sum_{n=0}^{m_0}(-1)^n d_n k^{2n} = k\sum_{n=0}^{n_0}(-1)^n c_n k^{2n}\tanh kh, \tag{A3}$$

with $f_0(y) = \frac{\cosh k_0(h-y)}{\cosh k_0 h}$. The bottom boundary condition is given by

$$\phi_y = 0 \quad \text{on } y = h. \tag{A4}$$

Finally, the velocity potential $\phi(x, y)$, on the vertical boundary at $x = 0$ satisfies the boundary condition

$$\phi(x, y) = u(y) \quad \text{on } x = 0. \tag{A5}$$

To derive the general form of the expansion formula for $\phi(x, y)$ satisfying (1) along with conditions (A1), (A4), and (A5) for $m_0 = n_0 = 2$, we substitute

$$\phi(x, y) = A_0 f_0(y)\mathrm{e}^{\mathrm{i}k_0 x} + \psi(x, y). \tag{A6}$$

Using the Fourier-sine transform of $\psi(x, y)$ as defined by

$$\hat{\psi}_s(\xi, y) = \int_0^\infty \psi(x, y)\sin\xi x\ \mathrm{d}x, \tag{A7}$$

we convert the BVP in $\psi(x, y)$ to a BVP of Sturm–Liouville type associated with an ordinary differential equation (ODE) in $\hat{\psi}_s(\xi, y)$. The solution of the ODE is derived by a Green's function technique and is given by

$$\hat{\psi}_s(\xi, y) = \frac{-S(\xi, y)}{H(\xi)}\int_0^h \cosh\{\xi(h-t)\}g(\xi, t)\mathrm{d}t - \frac{1}{\xi}\int_0^y \sinh\{\xi(t-y)\}g(\xi, t)\mathrm{d}t + \frac{\hat{f}(\xi)}{(d_0 - d_1 k_n^2 + d_2 k_n^4)}, \tag{A8}$$

where

$$S(\xi, y) = \xi(c_0 - c_1\xi^2 + c_2\xi^4)\cosh\xi y - (d_0 - d_1\xi^2 + d_2\xi^4)\sinh\xi y,$$

$$H(\xi) = \xi(c_0 - c_1\xi^2 + c_2\xi^4)\sinh\xi h - (d_0 - d_1\xi^2 + d_2\xi^4)\cosh\xi h,$$

$$g(\xi, y) = -\xi\{u(y) - A_0 f_0(y)\} + \xi^2\hat{f}(\xi)/\{(d_0 - d_1k_n^2 + d_2k_n^4)\},$$

$$\begin{aligned}\hat{f}(\xi) = {} & \xi(c_2\xi^2u'(0) + c_2u'''(0) - c_1u'(0)) + A_0k_0\xi\{c_2(\xi^2 + k_0^2) - c_1\}\tanh k_0h \\ & + \xi(d_2\xi^2u(0) + d_2u''(0) - d_1u(0)) + A_0\xi\{d_2(\xi^2 + k_0^2) - d_1\}.\end{aligned}$$

We observe, that $H(\xi) = 0$ has a real positive root at $\xi = k_0$ (say) which suggests that the function $\hat{\psi}_s(\xi, y)$ has a singularity at $\xi = k_0$ on the positive real axis. However, $\hat{\psi}_s(\xi, y)$ being the Fourier-sine transform of a function that cannot have a singularity on the line $\xi > 0$, this yields

$$\lim_{\xi \to k_0}(\xi - k_0)\hat{\psi}_s(\xi, y) = 0. \tag{A9}$$

Simplification of Eq. (A9) gives rise to the constant A_n with $n = 0$; this is given by

$$\begin{aligned}A_n = {} & \frac{1}{C_n}\int_0^h u(t)f_n(t)\,\mathrm{d}t + \frac{1}{C_n(d_0 - d_1k_n^2 + d_2k_n^4)}[\{-c_2u'''(0) + (c_1 - c_2k_n^2)u'(0)\}k_n \\ & + \{-d_2u''(0) + (d_1 - d_2k_n^2)u(0)\}k_n]\tanh k_nh\end{aligned} \tag{A10}$$

with

$$C_n = \frac{h}{2\cosh^2 k_nh} + \frac{(c_0 - 3c_1k_n^2 + 5c_2k_n^4)\tanh k_nh}{2k_n(c_0 - c_1k_n^2 + c_2k_n^4)} + \frac{(d_1 - 2d_2k_n^2)}{(c_0 - c_1k_n^2 + c_2k_n^4)}. \tag{A11}$$

Fourier-sine inversion of $\hat{\psi}_s(\xi, y)$ yields

$$\psi(x, y) = \frac{2}{\pi}\int_0^\infty \hat{\psi}_s(\xi, y)\sin\xi x\mathrm{d}\xi. \tag{A12}$$

Next, by writing $\sin\xi x$ as $(\mathrm{e}^{\mathrm{i}\xi x} - \mathrm{e}^{-\mathrm{i}\xi x})/2\mathrm{i}$ in (A12), we rotate the contour along the positive imaginary axis for the integral involving $\mathrm{e}^{\mathrm{i}\xi x}$ and along the negative imaginary axis for the integral involving $\mathrm{e}^{-\mathrm{i}\xi x}$. Then, using the Cauchy residue theorem of complex-function theory, we can rewrite (A12) as

$$\psi(x, y) = A_I f_I(y)\mathrm{e}^{\mathrm{i}k_Ix} + A_{II}f_{II}(y)\mathrm{e}^{-\mathrm{i}k_{II}x} + \sum_{n=1}^{\infty} A_n f_n(y)\mathrm{e}^{-k_nx}, \tag{A13}$$

where A_I, A_{II} and A_n are as in (A10) with $k_n = k_n$ for $n = I, II$ and $k_n = \mathrm{i}k_n$ for $n = 1, 2, \ldots$. Substituting for $\psi(x, y)$ from relation (A13) and A_n from relation (A10) in the relation (A6), the required expansion formula is obtained.

NB: It may be noted that the f_n satisfy the orthogonal mode-coupling relation as given by

$$\begin{aligned}\langle f_n(y), f_m(y)\rangle = {} & \int_0^h f_n(y)f_m(y)\mathrm{d}y - \frac{c_{j1}f_n'(0)f_m'(0)}{(d_{j0} - d_{j1}k_{jn}^2 + d_{j2}k_{jn}^4)} + \frac{c_{j2}\{f_n'(0)f_m'''(0) + f_n'''(0)f_m'(0)\}}{(d_{j0} - d_{j1}k_{jn}^2 + d_{j2}k_{jn}^4)} \\ & + \frac{d_{j1}f_n(0)f_m(0)}{(c_{j0} - c_{j1}k_{jn}^2 + c_{j2}k_{jn}^4)} - \frac{d_{j2}\{f_n'(0)f_m''(0) + f_n''(0)f_m'(0)\}}{(c_{j0} - c_{j1}k_{jn}^2 + c_{j2}k_{jn}^4)}\end{aligned} \tag{A14}$$

with

$$\langle f_n(y), f_m(y)\rangle = \begin{cases} 0 & \text{for } m \neq n, \\ C_n & \text{for } m = n. \end{cases} \tag{A15}$$

The above mode-coupling relation is a generalization of the one discussed in [6] and is equivalent to that derived by Lawrie and Abrahams [21]. It may be noted that the general expansion formulae can be derived in a straightforward manner once the root behavior of the dispersion relation as in (A3) is known.

Acknowledgements JB acknowledges the financial support received from CSIR, New Delhi and NBHM, DAE, Government of India in terms of senior research fellowship and post doctoral fellowship. The work is partially supported by Naval Research Board, New Delhi.

References

1. Greenhill AG (1887) Wave motion in hydrodyanamics. Am J Math 9:62–112
2. Williams TD, Squire VA (2004) Oblique scattering of plane flexural-gravity waves by heterogeneities in sea-ice. Proc R Soc Lond A 460(2052):3469–3497
3. Fox C, Squire VA (1994) On the oblique reflection and transmission of ocean waves at shore fast sea ice. Phil Trans R Soc Lond A 347:185–218
4. Sahoo T, Yip TL, Chwang AT (2001) Scattering of surface waves by a semi-infinite floating elastic plate. Phys Fluid 13(11): 3215–3222
5. Evans DV, Porter R (2003) Wave scattering by narrow cracks in ice sheets floating on water of finite depth. J Fluid Mech 484: 143–165
6. Manam SR, Bhattacharjee J, Sahoo T (2006) Expansion formulae in wave structure interaction problems. Proc R Soc Lond A 462(2065):263–287
7. Watanabe E, Utsunomiya T, Wang CM (2004) Hydroelastic analysis of pontoon-type VLFS: a literature survey. Eng Struct 26:245–256
8. Chen X, Wu Y, Cui W, Jensen JJ (2006) Review of hydroelasticity theories for global response of marine structures. Ocean Eng 33:439–457
9. Newman JN (1965) Propagation of water waves over an infinite step. J Fluid Mech 23(Part 2):399–415
10. Dingemans MW (1997) Water wave propagation over uneven bottoms, Part-I—Linear wave propagation. Advanced series on Ocean Engineering—vol 13, World Scientific
11. Berkhoff JCW (1972) Computation of combined refraction-diffraction. Proceedings of 13th International conference on Coastal Engineering. ASCE 1, pp 472–490
12. Rhee JP (1997) On the transmission of water waves over a shelf. Appl Ocean Res 19:161–169
13. Rhee JP (2001) A note on the diffraction of obliquely incident water waves by a stepwise obstacle. Appl Ocean Res 23:299–304
14. Ehrenmark UT (1998) Oblique Wave incidence on a plane beach: the classical problem revisited. J Fluid Mech 368:291–319
15. Sturova IV (2001) The diffraction of surface waves by an elastic platform floating on shallow water. J Appl Math Mech 65(1): 109–117
16. Wang CD, Meylan MH (2002) The linear wave response of a floating thin plate on water of variable depth. Appl Ocean Res 24:163–174
17. Andrianov AD, Hermans AJ (2002) Diffraction of surface waves by VLFP on water of infinite, finite or shallow depth. DAY on Diffraction, Proceedings, International seminar 5–8 June, pp 13–23
18. Williams TD, Squire VA (2006) Scattering of flexural-gravity waves at the boundaries between three floating sheets with applications. J Fluid Mech 569:113–140
19. Porter D, Porter R (2004) Approximations to wave scattering by an ice sheet of variable thickness over undulating bed topography. J Fluid Mech 509:145–179
20. Belibassakis KA, Athanassoulis GA (2006) A coupled-mode technique for weakly nonlinear wave interaction with large floating structures lying over variable bathymetry regions. Appl Ocean Res 28:59–76
21. Lawrie JB, Abrahams ID (1999) An orthogonality relation for a class of problems with high-order boundary conditions; Applications in sound-structure interaction. Q J Mech Appl Math 52(2):161–181
22. Magrab EB (1979) Vibrations of elastic structural members, SIJTHOFF and NOORDHOFF. Alphen aan den Rijn, The Netherlands
23. Wehausen JV, Laitone EV (1960) Surface waves. Encyclopedia of Physics, vol 9, Springer, Berlin, 9, pp 446–814. also at http://www.coe.berkeley.edu/SurfaceWaves (Accessed 1 Aug 2002)
24. Dean RG, Dalrymple RA (2001) Water wave mechanics for engineers and scientists. Allied Publishers Limited, World Scientific
25. Karmakar D, Bhattacharjee J, Sahoo T (2007) Expansion formulae for wave structure interaction problems with applications in hydroelasticity. Intl J Eng Sci 45:807–828